
Since January 2020 Elsevier has created a COVID-19 resource centre with free information in English and Mandarin on the novel coronavirus COVID-19. The COVID-19 resource centre is hosted on Elsevier Connect, the company's public news and information website.

Journal of Hazardous Materials 439 (2022) 129697

Contents lists available at ScienceDirect

Journal of Hazardous Materials

journal homepage: www.elsevier.com/locate/jhazmat

Research Paper

# Ventilation reconstruction in bathrooms for restraining hazardous plume: Mitigate COVID-19 and beyond

Ji-Xiang Wang [a,b,*], Zhe Wu [a], Hongmei Wang [a], Mingliang Zhong [c], Yufeng Mao [c], Yunyun Li [d], Mengxiao Wang [e], Shuhuai Yao [b,f,**]

[a] College of Electrical, Energy and Power Engineering, Yangzhou University, Yangzhou 225009, PR China
[b] Department of Mechanical and Aerospace Engineering, The Hong Kong University of Science and Technology, Clear Water Bay, Kowloon, Hong Kong, PR China
[c] Institute of Optics and Electronics, Chinese Academy of Sciences, Chengdu 610209, PR China
[d] School of Energy and Environment, Southeast University, Nanjing 210096, PR China
[e] Department of Traditional Chinese Medicine, Tianjin Medical University General Hospital, Tianjin 300052, PR China
[f] Department of Chemical and Biological Engineering, The Hong Kong University of Science and Technology, Clear Water Bay, Kowloon, Hong Kong, PR China

## HIGHLIGHTS

- Traditional ceiling fan fails to remove hazardous plume in bathrooms.
- Ventilation deficiency should be responsible for the vertical COVID transmission.
- A side-wall fan has the most efficient aerosol removal capability.
- In-site experimental conclusions were coherent with the simulation ones.
- Bathroom ventilation reconstructions are encouraged to be performed accordingly.

## GRAPHICAL ABSTRACT

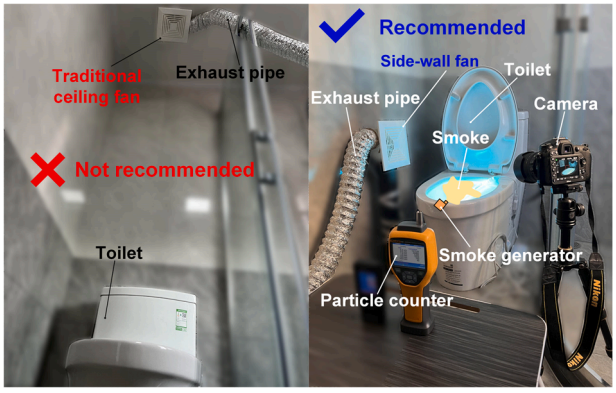


## ARTICLE INFO

Editor: Dr. R Teresa

*Keywords:*
Disease control and prevention
Public health
Indoor environments
Ventilation systems
Human hygiene

## ABSTRACT

Converging evidence reports that the probability of vertical transmission patterns via shared drainage systems, may be responsible for the huge contactless community outbreak in high-rise buildings. Publications indicate that a faulty bathroom exhaust fan system is ineffective in removing lifted hazardous virus-laden aerosols from the toilet bowl space. Common strategies (boosting ventilation capability and applying disinfection tablets) seem unsustainable and remain to date untested. Using combined simulation and experimental approaches, we compared three ventilation schemes in a family bathroom including the traditional ceiling fan, floor fan, and side-wall fan. We found that the traditional ceiling fan was barely functional whereby aerosol particles were not being adequately removed. Conversely, a side-wall fan could function efficiently and an enhanced ventilation

* Corresponding author at: College of Electrical, Energy and Power Engineering, Yangzhou University, Yangzhou 225009, PR China.
** Correspondence to: Department of Mechanical and Aerospace Engineering, The Hong Kong University of Science and Technology, Kowloon, Hong Kong, PR China.
*E-mail addresses:* mejxwang@ust.hk (J.-X. Wang), meshyao@ust.hk (S. Yao).

https://doi.org/10.1016/j.jhazmat.2022.129697
Received 20 May 2022; Received in revised form 11 July 2022; Accepted 27 July 2022
Available online 29 July 2022

capability can have increased performance whereby nearly 80.9% of the lifted aerosol particles were removed. There exists a common, and easily-overlooked mistake in the layout of the bathroom, exposing occupants to a contactless vertical pathogen aerosol transmission route. Corrections and dissemination are thus imperative for the reconstruction of these types of family bathrooms. Our findings provide evidence for the bathroom and smart ventilation system upgrade, promoting indoor public health and human hygiene.

## 1. Introduction

The Severe Acute Respiratory Syndrome Coronavirus 2 (SARS-CoV-2) and its variants have been raging across the world for more than two years since 2020 due to its highly transmissible infectivity (Lu et al., 2020; Kanso et al., 2020). Here the air-borne droplet or aerosol (Mirzaie et al., 2021; Zheng et al., 2021), and contact (Liu et al., 2022; Yu et al., 2021) transmissions have been identified as the major routes for causing cross-infection of coronavirus 2019 (COVID-19) among human populations (Kutralam-Muniasamy et al., 2022). Owing to enhanced

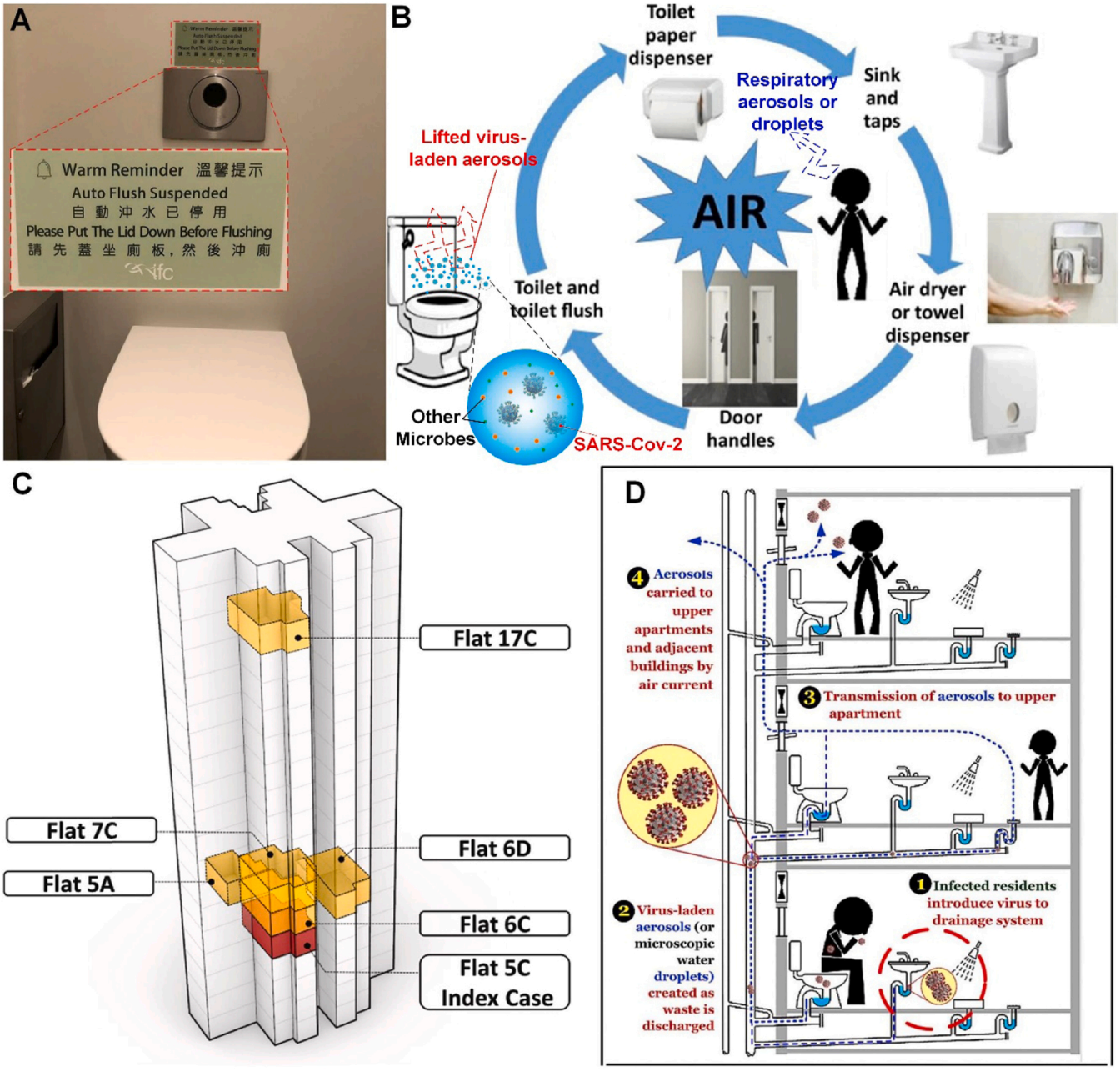


**Fig. 1.** Evidence for Covid-19 Transmission in bathrooms/restrooms. (A) Warning in public restrooms (Photographed in a public restroom in Victoria Peak, Hong Kong). (B) Disease transmission routes in restrooms or bathrooms (Adapted from Dancer et al., 2021's work) with an emphasis on the virus-laden droplet particle (Sizes of the virus in the droplet particle are not to scale). (C) Evidence of chimney-effect-induced cross-infection of COVID-19 in real-world examples: infected case distribution in the Kensington Plaza, Hong Kong (The image is originally from Wang et al., 2022b's work). (D) Detailed mechanism of chimney effect where viruses could be lifted into the air by upward flow movement (Adapted from Tran et al., 2021's work).

concentrations of virus-laden air-borne droplets or aerosols, confined indoor or built environments such as hospital wards (Feng et al., 2021; Huang et al., 2022; Kong et al., 2021; Park et al., 2022a), elevators (Dbouk and Drikakis, 2021; Park et al., 2022b), restaurants (Cheng et al., 2022b; Li et al., 2021; Wu et al., 2021), bus spaces (Cheng et al., 2022a; Mesgarpour et al., 2021; Yang et al., 2020; Yao and Liu, 2021), etc. with poor ventilation are indoor spaces with high probabilities of COVID-19 cross-infection. Besides this, increasing attention has also been paid to transmission mechanisms in indoor bathrooms or restrooms (Wang and Liu, 2021). Here Liu et al. (2020) have demonstrated that RNA concentrations of SARS-CoV-2 in air environment of the bathroom used by confirmed COVID-19 cases were higher than those in the isolation and ventilation wards although they do spend less time in bathrooms (Liu et al., 2020). In real life, there have been many reported cross-infection cases within restrooms and bathrooms. In Guangzhou, China, the index case (Delta carrier) and the secondary case entered a public restroom in one after another, and spent nearly one and a half minute together when the virus cross-infection happened (Breaking Latest News, 2021). A similar case took place almost instantly in just 14 s, indicating a contactless infection in the public restroom (Breaking Latest News, 2021). Such cross-infection cases were also reported in public bathrooms in Beijing, China (Global Times, 2020) as well as in a commercial airplane toilet (Cable News Network, 2020).

Various common human activities may be causes for massive cross-infections in indoor bathrooms and restrooms. Li et al. (2020), Wu et al. (2020), and Wang et al., 2020a, reported that water flushing in toilets and urinals could raise virus-laden aerosols, which may cause indoor cross-infections. They have thus recommended closing the toilet bowl lid before flushing to prevent this. As shown in Fig. 1A, posters and warnings like “Auto Flush Suspend. Please Put The Lid Down Before Flushing” have been posted in public restrooms or announced in Covid-19 prevention manuals across the world, which infers that governments and policy-makers have been attaching great importance to the prevention of COVID-19 transmission in restrooms and bathrooms. Schreck et al. (2021) believed that closing the lid alone, however, is not enough for reducing disease transmission as the lid may not be sufficiently a barrier for the small droplet-induced aerosolization risks. They proposed that ventilation enhancements would be a promising approach to lower the level of both flush-generated and respiratory aerosols to a minimum. However, bathrooms or restrooms are often identified as poorly-ventilated areas. Besides flushing, urination can also raise hazardous biomatter from the toilet bowl, as has been found by Cao et al. (2022), more recently. The turbulence-induced disturbance is thought to be responsible for the mass-scale spread of SARS-CoV-2 (Bourouiba, 2020, 2021; Bourouiba et al., 2014). In general, two main transmission mechanisms, shown below in Fig. 1B, in restrooms or bathrooms have been summarized by Dancer et al. (2021): (1). Airborne transmission via respiratory aerosols (droplets), fecal- and/or urinary-shedding aerosols (Guo et al., 2021; Peng et al., 2020), and (2). fomite transmission via frequent touch sites, which are shown in Fig. 1B, formed as a cycle of transmission.

Even more compellingly, typical family bathroom-related community outbreaks of COVID-19 in high-rise buildings in Hong Kong were investigated by Wang et al. (2022b). As demonstrated in Fig. 1C, most secondary infected cases lived in vertically aligned apartments (flats) (Flats 6 C, 7 C, and 17 C) above the index case flat (Flat 5 C), where these flats shared the same drainage system in bathrooms. Further on-site measurements were conducted where tracer gas (to simulate the movement of infectious virus-laden aerosols) was released into the drainage system in Flat 5 C (the index case flat/site of the first infection) and subsequently, the gas was detected by detectors in Flats 6 C, 7 C, 17 C, 10 C, and their roof vents. For gas detection in these flats, the detectors were placed above the toilet bowls in the corresponding flat bathrooms. It was believed here that infectious virus-laden aerosols could be transmitted across floors by common human behaviors in bathrooms, and known as the chimney effect (Wang et al., 2022b). A detailed schematic mechanism of the chimney effect is shown in Fig. 1D where the virus-laden aerosols in drainage stack can be generated during the discharge of domestic wastewater containing urine, fecal-matter, and exhaled mucus particles when the index case used their toilets and washbasins. Thus, an upward airflow caused by a density difference (a buoyancy flow) would have a high-probability of bringing virus-laden particles upwards to the floors above. Finally, these hazardous particles would be spread to other vertical indoor bathrooms via toilet bowls there because of the chimney effect. It has been recognized that chimney-effect-induced hazardous plume may be responsible for multiple COVID-19 community outbreaks in Hong Kong (Wang et al., 2022b, 2022c). Ali et al. (2021) and Wade et al. (2022) cross-confirmed that drainage systems contain a considerable number of infective viruses, which suggests a critical significance of the chimney effect to public health. Besides the cases in Hong Kong, cross-infections in vertically-aligned family bathrooms of high-rise buildings have been identified worldwide such as Guangzhou (Kang et al., 2020) and Seoul (Hwang et al., 2021). Most recently, contactless infections were reported suspected to be caused by the shared drainage system in the bathroom in the latest outbreak of Omicron in Shanghai (Tencent News, 2022). Therefore, COVID-19 prevention measurements should be highlighted in every single bathroom. This is also not limited to SARS-CoV-2, similar cross-infection clusters caused by SARS-CoV also in a vertical column of apartments/flats occurred in the now notorious high-rise building, Amoy Gardens, in Hong Kong where the SARS crisis began, and where as many as three hundred people were infected (Yu et al., 2004).

Adequate air ventilation is essential for reducing COVID-19 transmission indoors (ASHRAE, 2020; Tang et al., 2021). Almost all the experts who concern themselves with COVID-19 transmission in bathrooms and restrooms including Wang et al. (2022b) and (2022c), Dancer et al. (2021), Wang and Liu, 2021, Kang et al. (2020), and Wang et al. (2021a), have proposed that ventilation enhancement in bathrooms or restrooms could fundamentally suppress family-bathroom-related or public-restroom-related infection cases. As investigated by Wang et al. (2022b), tracer gas used to evaluate this could be also detected even when exhaust fans in bathrooms were switched on, indicating a faulty ventilation approach in the family bathroom environment. However, there are few publications concerning specific ventilation improvement in bathrooms or restrooms for the purpose of minimizing chimney-effect-induced hazardous plumes from toilet bowls, exposing millions of people to the vertical transmission of airborne pathogens. To support this there is plenty of research on ventilation optimization in other indoor environments. For example, Peng et al. (2022) proposed methods to increase ventilation rates to enhance the aerosol-removal rates, which could decrease cross-infections in shared rooms. Wang et al. (2022a) developed an on-line smart ventilation system which can control ventilation according to human activities. Results indicates that the cross-infection probability can be reduced by 4.30–6.30% and the consumed energy can be decreased by 13.0%. It shows that the ventilation flow rate does play an important role in the indoor infection control. Moritz et al. (2021) reported a successful deployment of a ventilation system in an arena where the location of exhaust towers was significant. This effective scheme was to place exhaust towers in the corners of the arena. Results also showed that a faulty ventilation system where the exhaust outlet was placed on the roof could have a ten-fold increase in the number of individuals exposed to infectious aerosols compared to the current successful air distribution approach. However, Wang et al. (2021b) suggested a bottom-in and top-out air ventilation in hospital wards as this would confine most of the airborne aerosols to the ceiling area, which could reduce the cross-infection possibilities among patients. Here it was suggested that roof exhaust outlets were preferable in relatively small confined indoor areas. One particularity of the bathroom space was identified that it only has an exhaust outlet without any air inlets. The peculiarity of the ventilation in bathrooms thus needs to be explored further. Seller et al. investigated natural draft ventilation

within a bathroom-bedroom environment with dispersion rates of PM 2.5 and PM 10 (Seller et al., 2021). Here it was found that opening the bathroom window could reduce PM concentrations significantly, but unfortunately increase the PM particle flow from the bathroom to the bedroom. Similarly, bathroom-borne virus aerosols could also be transported to other indoor spaces in a poor ventilated condition, which would cause mass cross-infections in shared houses or apartments/flats. From literature review, there are few articles involving into aerosol-coupled ventilation systems in bathrooms. Currently, there are only general untested measures such as boosting ventilation capability to prevent COVID-19 infection in bathrooms. Considering the huge risks of bathroom-related infection via vertical transmission patterns, there is an urgent need for an air distribution optimization system in bathrooms to create a healthier built environment.

In this paper, we both quantitatively and visually demonstrate the effects of ventilation airflow speed, fan locations, and fan size on the distribution of virus aerosols in a typical family bathroom. As shown in Fig. 2, combined approaches of computational fluid dynamics (CFD) and family bathroom-based smoke-assisted experiments were used to explore multi-phase airflow dynamic characteristics. In our simulation, the *Euler-Lagrangian Method* was adopted to characterize the flow dynamics, aerosol escape rate, and aerosol-air interactions within a family-based bathroom. The computational domain and its structure, shown in Fig. 2A, was based on a typical family bathroom as demonstrated in Fig. 2B. The effects of the ventilation airflow speed, exhaust fan locations (Schemes I, II, and III), and fan size on the distribution of aerosol particles in the bathroom space were studied. This illustrated how airflow patterns contribute to or suppress the spread of aerosols within the bathroom and the aerosol escape ratio through the bathroom door. Conclusions from simulation were validated with experiments in which a smoke generator and a particle counter (shown in Fig. 2D) were used to visualize the flow dynamic distribution and measure particle concentration under two selected ventilation systems (Fig. 2C shows the ceiling fan arrangement and Fig. 2D displays the side fan). Results in this paper have identified an optimal ventilation approach where both aerosol concentration and escape rate could be suppressed to a minimum. The uniqueness of this paper lies in the challenge to the traditional ventilation arrangement and proposes an optimal bathroom ventilation with solid data evidence. This paper thus contributes to knowledge in creating a safe and healthy indoor built environment, minimizing chimney-effect-induced vertical transmissions in family bathrooms and public restrooms, and preparing human occupants better for emerging and re-emerging pandemics from community units that may occur in the future.

## 2. Methods

### 2.1. Spatial methods

As shown in Fig. 2, this paper targets a typical family bathroom. A

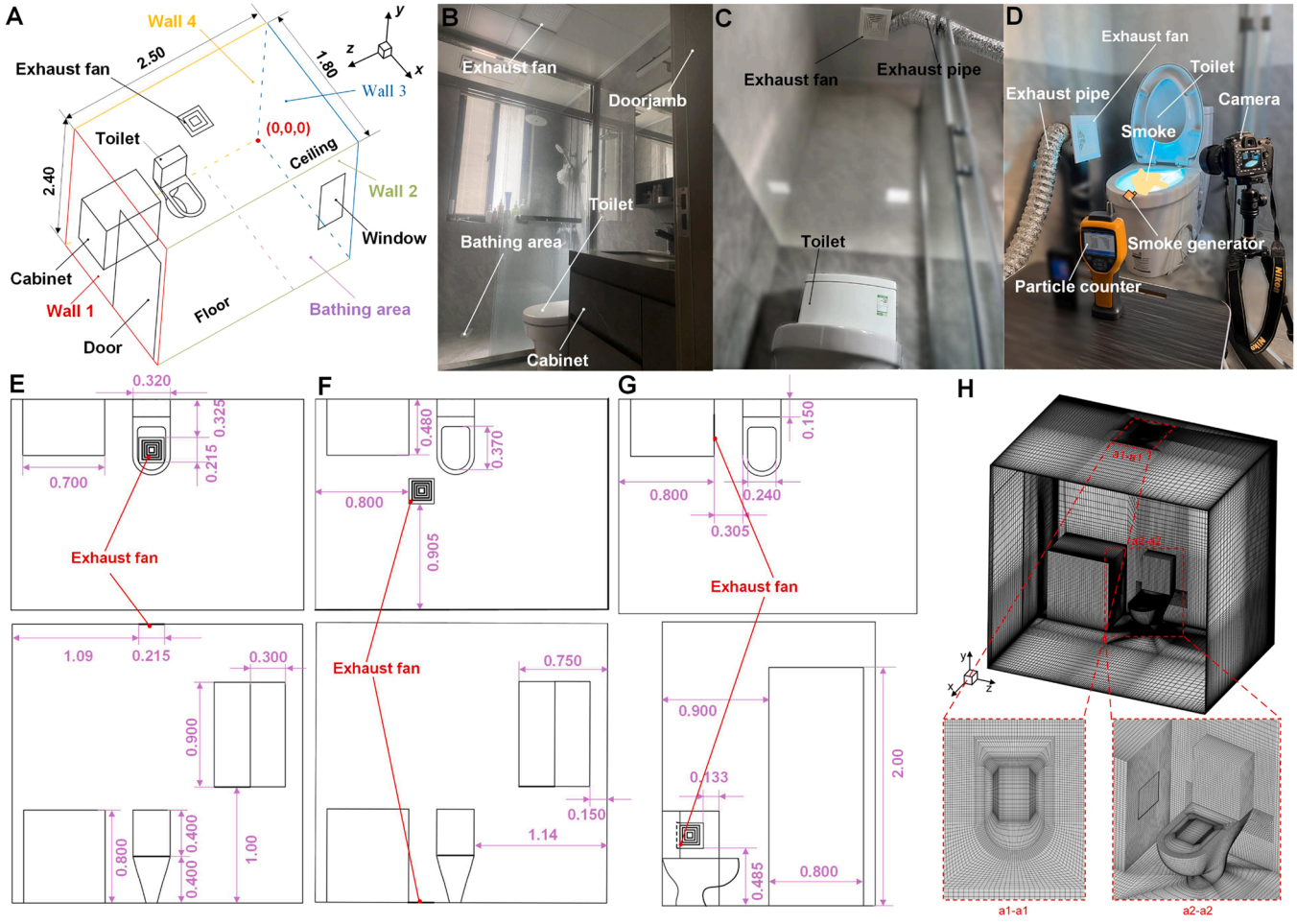


**Fig. 2.** Simulation and experimental framework. (A) Structure and overall size of the computational domain of a family bathroom with the red dot representing the coordinate origin. (B) Practical counterpart of the computational domain. (C) Ventilation experiment with the fan on the ceiling (Scheme I). (D) Photographic view of the smoke-assisted ventilation experiment with the fan on the side of the toilet (Scheme III). (E) Geometric dimensions of the traditional ventilation scheme (Scheme I). (F) Geometric dimensions of the floor ventilation scheme (Scheme II). (G) Geometric dimensions of the side ventilation scheme (Scheme III). (H)Typical domain discretization for Schemes III with a standard fan.

typically sized family bathroom with the dimensions (length × width × height) of 2.50 m × 1.80 m × 2.40 m was selected as the object in which traditional ventilation and improved versions were presented and compared. The four walls of the bathroom are categorized as Wall 1, Wall 2, Wall 3, and Wall 4. An unlocked door is also emplaced in Wall 1 and its width and height are 0.800 m and 2.00 m. A semi-open window, located in the bathing area, is emplaced in Wall 2 with a width × height of 0.600 m × 0.900 m. The test is a toilet in the middle of the bathing area and a cabinet nearby mounted on Wall 4 and close to Wall 1. The distance between the cabinet and wall 1 is 0.100 m. As a traditional ventilation scheme, the exhaust fan is located in the ceiling, which is directly above the toilet.

Fig. 2E–G present three different ventilation schemes with detailed geometric sizes in which Fig. 2E–G respectively illustrate the traditional ventilation scheme (marked by scheme I), the floor ventilation scheme (marked by scheme II), and the cabinet side ventilation scheme (marked by scheme III). In Fig. 2E, the exhaust fan is installed on the ceiling above the toilet. Scheme II shows a bottom-out scheme where the fan is placed on the floor near the toilet. The distances between this fan and Walls 1 and 2 are 0.800 m and 0.905 m respectively. The distance between the fan and the toilet bowl is 0.400 m. As shown in Fig. 2G, the exhaust fan is located on the sidewall of the bathroom cabinet near the toilet where the distance between the fan and the toilet is 0.305 m and the height of the fan from the floor is 0.485 m. In this paper, a standard family bathroom fan of 0.215 m × 0.215 m and a large fan of 0.430 m × 0.430 m were used with the center coordinates for these two fans the same in each selected ventilation scheme. Besides, a human was incorporated in the Scheme III which is marked by Scheme III.I in this paper. Please refer to Supplementary materials, Section S1 for detailed descriptions of Scheme III.I.

### 2.2. Modeling methods

The CFD approach was adopted to simulate the airflow and aerosol movements in the test bathroom. The three-dimensional model for this bathroom was constructed by the software of Solidworks 2021. Subsequently, a computational domain discretization was conducted in ICEM 2019. The total number of the hybrid (structured and unstructured) grids (in Fig. 2H) passed the grid independence test, was 1,460,155 (average grid size: 17.3 mm × 20.8 mm×22.0 mm). (See Section 2.3 for detailed results of the grid independence test) Within the simulation framework, the transient time-averaged *Navier-Stokes Equation* with a realizable $k$-$\varepsilon$ model (Shih et al., 1995) was adopted as the momentum conservation equation to simulate the overall airflow within the computational domain. Such a model has already been applied successfully to the airflow within hospital wards (Wang et al., 2021b) and many other building indoor space (Sheikhnejad et al., 2022). Besides this method, the mass conservation, energy conservation, and species transport equations were also used in the model. Aerosol particle trajectories were tracked by a discrete phase model (DPM), which was also been previously applied to flushing-caused plume microbe particle path simulations (Li et al., 2020), cough-induced droplet particle tracking (Dbouk and Drikakis, 2020) as well as other much complex droplet processes (Wang et al., 2020b, 2021c). (See Supplementary materials, Section S2 for the detailed governing equations).

In the simulation framework, the indoor temperature was maintained at 22 °C. The temperature of the incoming wind from the window was set 22 °C. The relative humidity was set at 60.0%. The semi-opened window was evaluated as a pressure inlet with a gauge pressure of 0 Pa, whilst the door was evaluated as a pressure outlet with a gauge pressure of - 4 Pa to form a 4 Pa indoor-outdoor pressure difference (Catalina et al., 2020). Thus we simulated a common condition that wind is driven into the bathroom and out again through the doorway. The toilet's outer surfaces (except the toilet seat plane), cabinet surfaces, bathroom walls, and surfaces of the incorporated human surfaces were treated as non-slip boundary conditions. For Scheme III.I, the metabolic rate of the incorporated human was set to be 58 W/m$^2$ (ASHRAE, 2013), and half of the heat (29 W/m$^2$) was considered to be dissipated from the human surfaces (Yu et al., 2017). In the DPM, all the surfaces were set to be a "trap" boundary condition. The toilet seat plane was regarded as a velocity inlet, which functioned to lift the released aerosol particles into the immediate atmosphere. The velocity data for the airflow from the toilet seat plane were determined to be 0.123 m/s (y direction), as measured during our experiments (See Supplementary materials, Section S3). The sizes of the aerosol particles are Rosin-Rammler-distributed with an average aerosol particle diameter of 5.0 μm (Fennelly, 2020) (maximum diameter: 10 μm, minimum diameter: 1.0 μm, and spread parameter: 8 (Dbouk and Drikakis, 2020)) and a density of 1.10 × 10$^3$ kg/m$^3$ (Li et al., 2020). Detailed aerosol particle release conditions are illustrated in Fig. 3. As shown in Fig. 3A, thirty particle release sources are normally distributed along the test toilet seat plane (shown in purple). Tails of these arrows in Fig. 3A. demonstrated locations of these particle release sources. The up arrow indicates the direction of the initial velocity. The initial velocity for each released particle was set to be 1.00 × 10$^{-5}$ m/s, which means the particle can only be lifted by the up-ward airflow from the toilet seat plane. Meanwhile, the total particle flow rate for each particle release source was set to be 6.50 × 10$^{-20}$ kg/s. That value can control the total released particle number. The total released aerosol particle number in this study was controlled to be 320. Exact coordinates of the total of thirty particle release sources are presented in Fig. 3B.

The fan in all the schemes was set to be a velocity inlet, where different velocities were then selected for analysis. For the standard fan, three velocities were selected: - 0.325, - 0.650 and - 1.30 m/s, which represents volume flow rates of 0.018, 0.030 and 0.060 m$^3$/s, respectively. The negative sign in the velocities indicated an exhaust fan. For a large fan, two velocities were also selected: - 0.325 and - 0.650 m/s, which represented 0.060 and 0.12 m$^3$/s, respectively. Air change rates per hour (ACHs) for these four volume flow rates (0.018, 0.030, 0.060 and 0.12 m$^3$/s) were 6, 10, 20, and 40 h$^{-1}$. Note that the selected ACHs were subject to the Chinese National Residential Ventilation Design Standard (T/CSUS 02–2020) and ASHRAE. Table 1 outlines the operating conditions of the simulation cases in this paper.

We adopted the pressure-implicit with splitting operator solution to calculate the coupling between pressure and velocity. Spatial discretization of the gradient, pressure, momentum, and volume fraction were selected respectively to be least-squares cell-based, PRESTO, second-order upwind, and geo-reconstruct. Spatial discretization of other variables such as turbulent kinetic energy and turbulent dissipation rates were assessed as second-order upwind. The time step size was 0.05 *s*, which could have a relatively rapid convergence. Solutions to the numerical model were conducted by ANSYS-FLUENT 19.2. Convergence criterion were set to be the absolute error of 10$^{-5}$ between the two consecutive iterations for all variables.

The processes of the simulation for each case condition and each scheme are identical for comparative study. Detailed processes sequences can be given as follows: (1). Use of the continuous model and turbulent model to simulate the airflow patterns for 60 s to establish a steady-state of airflow pattern in the test bathroom (with no ascending air from the toilet seat plane); (2). Add the DPM at the elapsed time of 60 s where both aerosol particles and ascending air begin to ascend from the toilet seat plane and last for 1 s (to simulate a 1 s toilet flushing process); (3). Continue the simulation until all particles disappear from the test bathroom.

The assumptions adopted in this simulation were: (1). Relative humidity variations were considered negligible; (2). Aerosol particles were assessed as those after evaporation because evaporation could be ignored for droplet-based aerosol particles at the measured scales (Shao et al., 2021; Narayanan and Yang, 2021; Nicas et al., 2005); (3). virus-laden aerosols were treated as droplet-based particles. (4) Breathing and movements of the incorporated human in Scheme III.I was ignored.

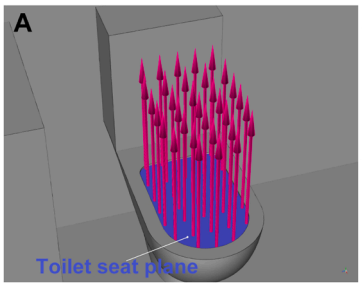


B (0.245, 0.400, 1.20) (0.380, 0.400, 1.19) (0.480, 0.400, 1.19)
(0.245, 0.400, 1.25) (0.380, 0.400, 1.25) (0.480, 0.400, 1.25)
(0.245, 0.400, 1.30) (0.380, 0.400, 1.30) (0.480, 0.400, 1.30)
(0.245, 0.400, 1.35) (0.380, 0.400, 1.36) (0.480, 0.400, 1.36)
(0.245, 0.400, 1.40) (0.380, 0.400, 1.41) (0.480, 0.400, 1.41)
(0.315, 0.400, 1.19) (0.430, 0.400, 1.19) (0.540, 0.400, 1.20)
(0.315, 0.400, 1.25) (0.430, 0.400, 1.25) (0.540, 0.400, 1.25)
(0.315, 0.400, 1.30) (0.430, 0.400, 1.30) (0.540, 0.400, 1.30)
(0.315, 0.400, 1.36) (0.430, 0.400, 1.36) (0.540, 0.400, 1.35)
(0.315, 0.400, 1.41) (0.430, 0.400, 1.41) (0.540, 0.400, 1.40)

**Fig. 3.** Detailed boundary condition for DPM. (A) Particle release illustration upon the toilet seat plane. The up arrows indicate the initial velocity direction of the released aerosol particles. (B) Detailed coordinates of thirty particle release sources which were treated as points (Unit: m).

**Table 1**
Operating conditions of the simulation cases.

| Case no. | Scheme | Fan size | ACH ($h^{-1}$) | Wind temperature (°C) | Indoor temperature (°C) | Relative humidity (%) |
|---|---|---|---|---|---|---|
| 1 | I | Standard | 6 | 22 | 22 | 60 |
| 2 | I | Standard | 10 | | | |
| 3 | I | Standard | 20 | | | |
| 4 | II | Standard | 10 | | | |
| 5 | II | Standard | 20 | | | |
| 6 | II | Large | 40 | | | |
| 7 | III | Standard | 6 | | | |
| 8 | III.I | Standard | 6 | | | |
| 9 | III | Standard | 10 | | | |
| 10 | III | Standard | 20 | | | |
| 11 | III | Large | 40 | | | |
| 12 | III.I | Large | 40 | | | |

### 2.3. Mesh sensitivity analysis

Mesh sensitivity analysis for Scheme I was conducted as shown in Fig. 4. Here four grid numbers were tested from the two perspectives of velocity and vorticity magnitude. Here it could be seen that when the grid number was less than 1,052,801, these simulation results could vary from one to the other. Once the grid number was above 1,460,155, the transient results from the two grid numbers were highly consistent. Therefore, a grid number of 1,460,155 was able to maintain both accuracy and computational economy. Although mesh sensitivity was conducted only for Scheme I, the other schemes also have the same dimensions with similar simulation settings. Thus, the mesh sensitivity results could also be applied to the other schemes in this paper.

### 2.4. Experimental methods

In-situ experiments were carried out in a typical family bathroom, as shown in Fig. 2C and D in which the two ventilation schemes (Scheme I shown in Fig. 2C and Scheme III as shown in Fig. 2D) for experimentation. For Scheme III, both standard (ACH was 10 $h^{-1}$) and large (ACH was 40 $h^{-1}$) fans were utilized in the experiments for Scheme III and only a standard fan (ACH was 10 $h^{-1}$) was adopted in the experiments for Scheme I. An airborne particle counter (Fluke 985) with a sample rate of 1 $s^{-1}$ and uncertainty of ± 1.00% was then adopted. This method has been verified in other research in that it can identify infectious aerosol particle type sizes (Cao et al., 2022). The distance between the test toilet center to the detected location was 0.6 m, and the height of the bowl was 0.600 m from the floor. A smoke generator (Gounengnai 400 W), was used to generate the smoke made from heated glycerol.

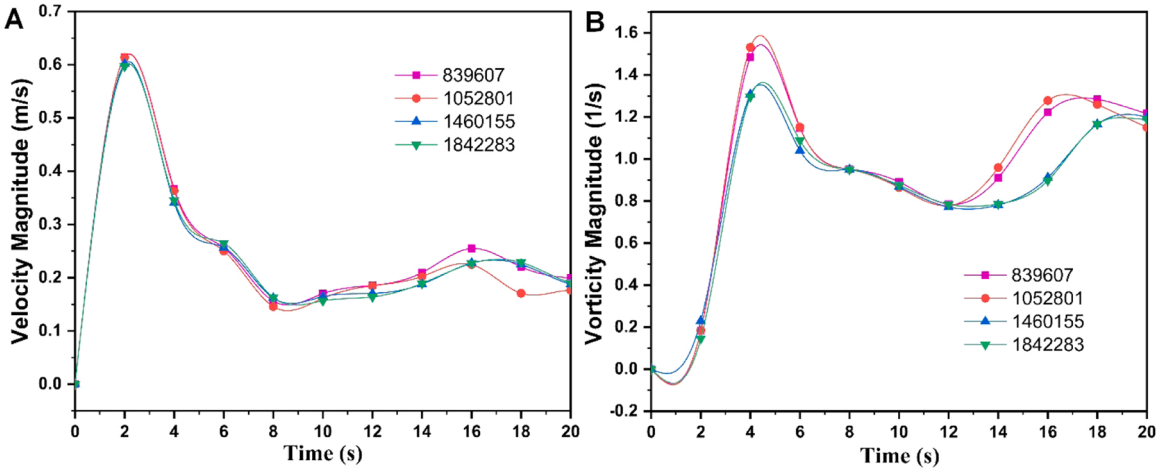


**Fig. 4.** Mesh sensitivity analysis of the model with the coordinate of (0.450, 1.50, 1.25) for Scheme I. (A) Mesh sensitivity analysis from the velocity perspective. (B) Mesh sensitivity analysis from the vorticity perspective.

Alongside this, a circular band light was placed on the internal wall of the bathroom unit to enhance visualization of the airflow pattern. The Camera (a Nikon D7100) was used to record the full process of the smoke-assisted experiment and for macroscopic visualization of flow patterns under the different ventilation schemes. Detailed experimental procedures of visualization experiments of the flushing-induced smoke-assisted are described in Supplementary materials, Section S4.

## 3. Results

### 3.1. Simulation results

Overall airflow distribution of the traditional ventilation scheme (Scheme I) is shown in Fig. 5. Due to the indoor-outdoor pressure difference (4 Pa), an inward airflow from the window was formed, and then, scattered when impacting Wall 4 (see the plane of Z = 2.20 m in Fig. 5A and Y = 0.400 m in Fig. 5B). As shown in Fig. 5A, the red arrows indicate the horizontal flow pattern from the window, impacting the opposite wall. After hitting the wall (Wall 4), the airflow, as shown in Fig. 5B, is driven along the bathroom wall and discharged out of the bathroom space through the doorway, which can be considered the main draught. Comparisons of two ACHs (10 and 20 $h^{-1}$) are shown in Fig. 5C, where detailed airflow patterns and mechanisms could also be observed. In general, airflow patterns within the bathroom would not be changed significantly with the increase in the ACH. In Fig. 5C two large vortexes are generated horizontally for both ACHs. The upper vortex is driven by the exhaust fan and the lower vortex is caused by the draught effect. The horizontal draught leads to a strong and clear horizontal airflow in both ACHs, separating vortex 1 and cortex 2. This horizontal airflow would thus prevent the ascending aerosols from being caught by the exhaust fan flow. Besides, the purple arrows shown in Fig. 5C demonstrate that downward airflow trends to be above the toilet seat although the fan's suction effect drives the upper-layer air movement upwards. The downward airflow just above the test toilet seat and the upward flow caused by toilet flushing are found to lead to horizontal flows also. Although the exhaust fan is operating, clear horizontal airflows just above the toilet could be identified and such horizontal airflows could then be caught by the strong draught and finally flowed out of the bathroom via the doorway. It is believed that the such an air distribution design confounds the pandemic prevention as few aerosols flowing out of the toilet bowl (caused by the chimney effect) would be caught by the fan suction flow and most could be easily spread out of the

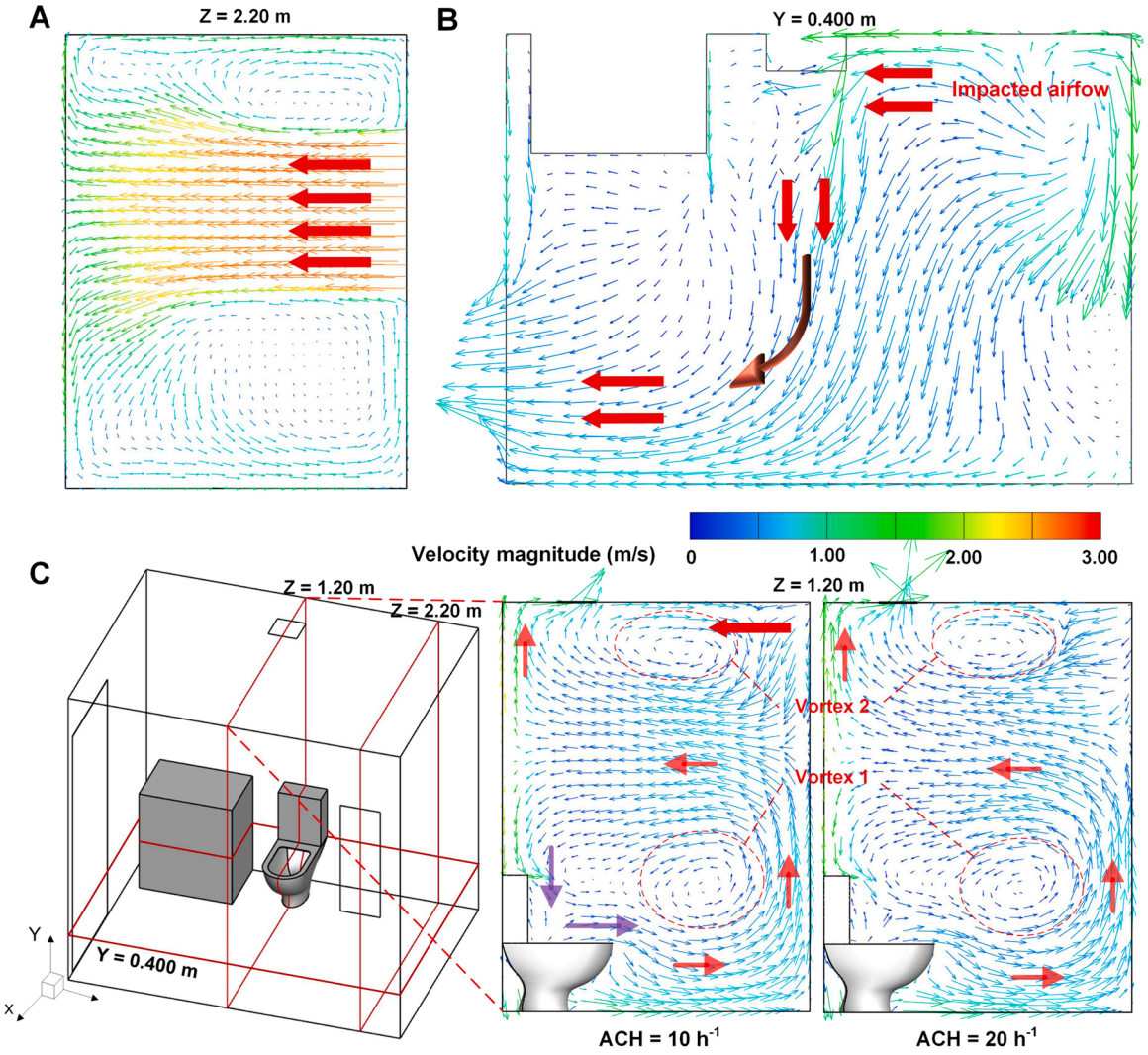


**Fig. 5.** Airflow pattern and aerosol movement dynamics. (A) Velocity vector field of airflows in planes of Y = 0.400 m and 1.48 m at ACH of 10 $h^{-1}$ using a standard fan. (B) Velocity vector field of airflows in planes of Z = 1.20 m and 2.20 m at ACH of 10 $h^{-1}$ using a standard fan. (C) velocity vector field of airflows in planes of X = 0.43 m and 1.30 m at ACH of 10 $h^{-1}$ using a standard fan. (D) Comparison of the velocity vector distribution for two different ACHs (10 and 20 $h^{-1}$) in the plane of Z = 1.20 m. (E) Aerosol particle movement at different time for the ACH of 10 $h^{-1}$. (F) Aerosol concentration in the bathroom versus times for two different ACHs (10 and 20 $h^{-1}$). (G) Comparisons of proportions of particles escaping from the fan and door for different ACHs.

bathroom and be a source for widespread infection.

Aerosol particle dynamic movements under the ACH of 10 $h^{-1}$ at different times ranging from 0.400 to 30.0 s are displayed in Fig. 6A where the process from particles ascending to spreading could be captured. In the first 5.00 s, most of the ascending particles were driven towards the door as shown in the red arrow in Fig. 6A. At a time of 10.0 s, the particles could be spread across the whole bathroom area. When time approaches 30.0 s, although the particle count is clearly diluted, viruses could still be distributed around the bathroom space. Particle concentration (PC) of the three ACHs (6, 10, and 20 $h^{-1}$) in the bathroom are plotted in Fig. 6B where the PC peak ($\sim 15.8 \times 10^{-24}$ kg/$m^3$) occurs at 1.00 s for all ACHs. Additionally, these three curves coincide with each other, showing an enhanced ventilation does not contribute well to virus-laden aerosol removal. Additionally, Fig. 6C shows that 100% of the escaped particles are escaping through the door when the ACHs are 6 or 10 $h^{-1}$, indicating a faulty ventilation fan. It would not help to simply boost the ACH as only 0.580% of the escape particles are captured by the fan when the ACH was increased to 20 $h^{-1}$ (See Movie S1 for the full process of the aerosol particle movement in Scheme I at ACH of 20 $h^{-1}$). It means that the PC dilution effect for all the three ACHs in Fig. 6B comes from the aerosol escaping from the door. Therefore, the traditional ventilation scheme (Scheme I) barely works as a barrier confronting the ascending virus-laden aerosols from the toilet space. In Scheme II, The ratios of the particles escaping from the fan to the total number of the released particles ($P_{ef}$) for the three ACHs of 10, 20, and 40 $h^{-1}$ are respectively 10.2%, 18.8%, and 30.8%, illustrating a huge improvement compared to Scheme I. Please refer to Supplementary materials, Section S5 for detailed description of simulation results of Scheme II.

Supplementary material related to this article can be found online at doi:10.1016/j.jhazmat.2022.129697.

Results of Scheme III are shown in Figs. 7 and 8 where airflow patterns of 40 $h^{-1}$ ACH are displayed in Fig. 7 and the aerosol particle movement dynamics are demonstrated in Fig. 8. As displayed in Fig. 7B, a strong suction effect flow (marked by blue arrows) occurs above the toilet bowl where the air is driven into the side fan. The red arrows in Fig. 7B show the main flow field of the air where the main draught still drives the air from the window to the door. Fig. 7C shows airflow velocity vector field and pressure distribution in the plane of Z = 1.20 m. The vortex above the toilet could drive the airflow along the x direction, which is consistent with the main flow in Fig. 7B. Besides, positive pressure above the toilet bowl, as shown in Fig. 7B could suppress the chimney-effect-induced aerosol plume. Fig. 7C manifests a large-scale draught-induced horizontal flow from the bathing area to Wall 1 as marked by the red arrows. Also, a clear suction flow from the near-toilet area to the fan could be observed as indicated by the blue arrows. Differing from the former two schemes, airflows near the toilet can be significantly extracted towards the fan.

Correspondingly, airborne aerosol particle dynamics results are improved significantly. Fig. 8A illustrated the particle movement dynamics under various ACHs (10, 20, and 40 $h^{-1}$). Compared to the other schemes above, generated aerosol particles tend to flow towards the fan at the first beginning for all three ACHs. At an elapsed time of 2.00 s, some of the aerosol particles escaped from the fan suction flow and moved along the x direction, which is consistent with airflow pattern analysis. When time elapsed approached 5.00 s, aerosols could still be spread throughout the bathroom space albeit with the particle density significantly diluted compared with that in the other ventilation schemes, suggesting an effective removal of ascending aerosols (See Movie S3 for full process of the aerosol particle movement in Scheme III at ACH of 40 $h^{-1}$). PCs in the bathroom space versus time for various ACHs are plotted in Fig. 8B. Before 1.00 s, PCs for various ACHs increase at an identical slope but the PC of 40 $h^{-1}$ with the large fan decreases at the fastest rate after 1.00 s. At the time of 10.0 s, the PC of 40 $h^{-1}$ with

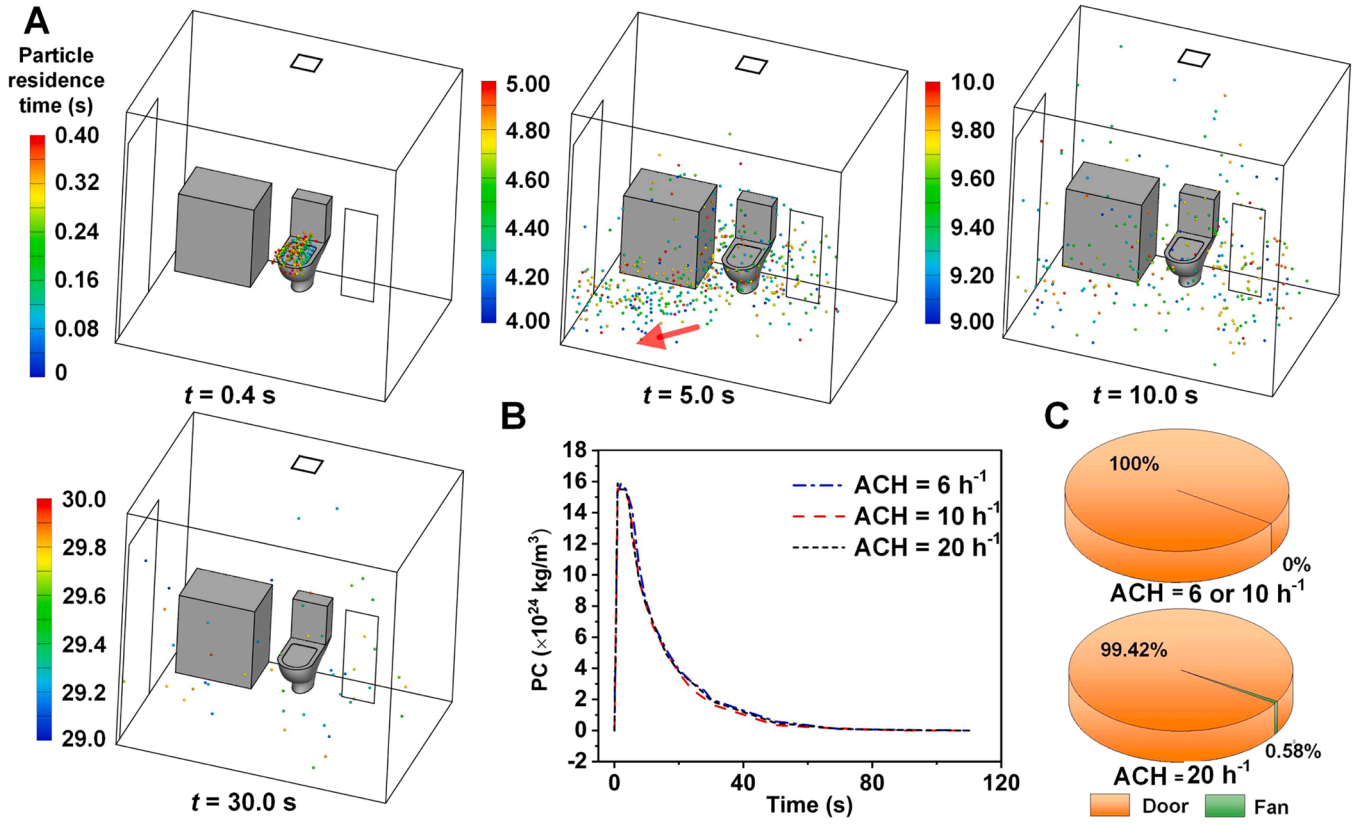


**Fig. 6.** Particle statistical results of Scheme I. (A) Aerosol particle movement at different time for the ACH of 10 $h^{-1}$. (B) Aerosol concentration in the bathroom versus times for two different ACHs (6, 10 and 20 $h^{-1}$). (C) Comparisons of proportions of particles escaping from the fan and door for different ACHs.

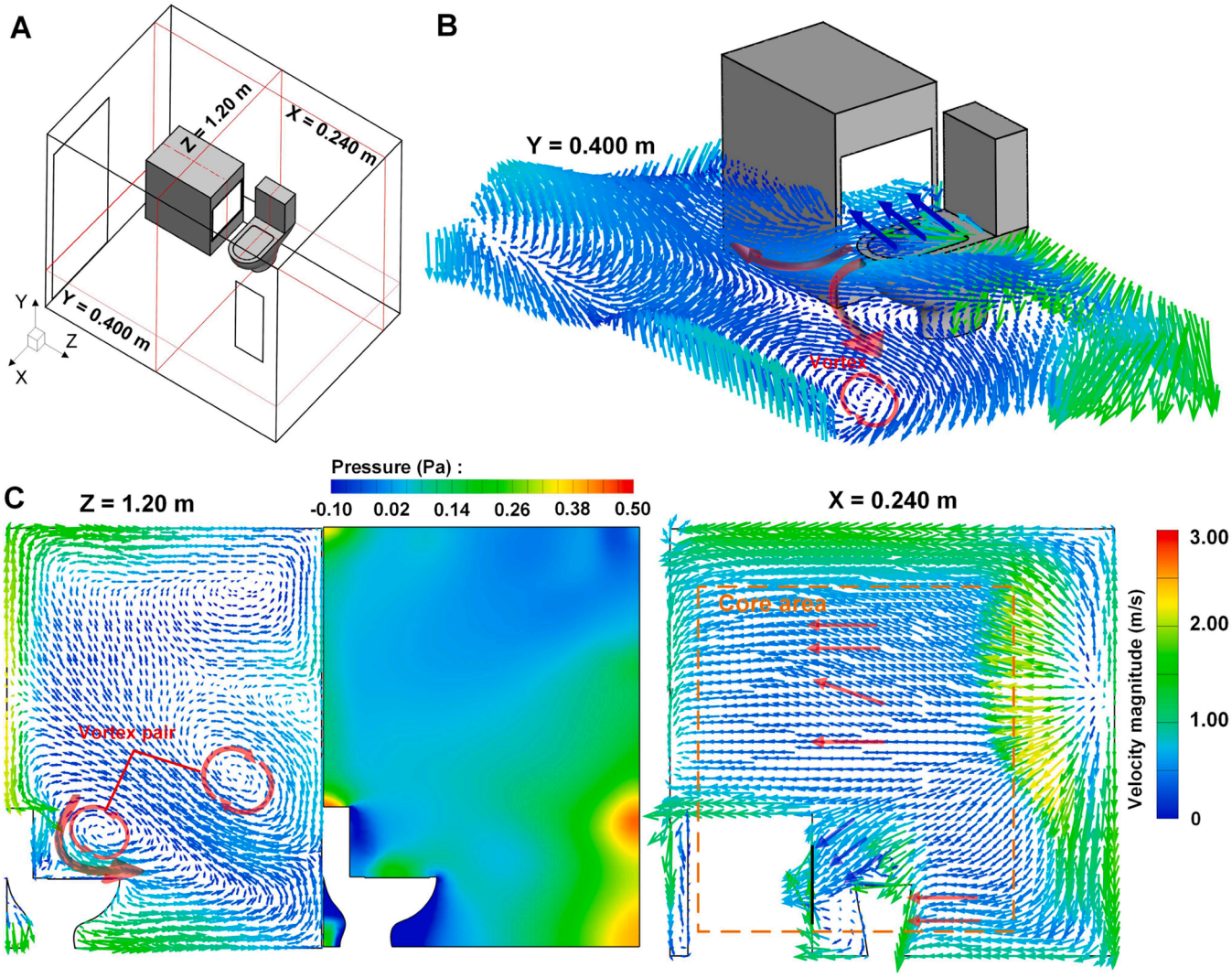


**Fig. 7.** Airflow pattern and pressure distribution of Scheme III at ACH of 40 $h^{-1}$ using a large fan. (A) Three focused surfaces identification. (B) Velocity vector field of airflows in the plane of Y = 0.400 m. (C) Airflow velocity vector field and pressure distribution in the plane of Z = 1.20 m. (D) Velocity vector field of airflows in the plane of X = 0.240 m.

the large fan is $2.20 \times 10^{-24}$ kg/$m^3$, while that of 10 $h^{-1}$ with the standard fan is $6.10 \times 10^{-24}$ kg/$m^3$. This means a three-fold enhanced ventilation capability can decrease PC by 64.0% in a time duration of 10.0 s. Fan-escaped particle ratio $P_{ef}$ for various conditions are displayed in Fig. 8C. The biggest ACH can bring the highest $P_{ef}$ where a 40 $h^{-1}$ can have a $P_{ef}$ of 80.9%. Similar to the results from Scheme II, an increase in ACH can bring a boost in $P_{ef}$. $P_{ef}$ can be elevated by 236% when ACH increases from 10 to 40 $h^{-1}$. Compared to the results for Scheme II under the same ventilation condition, the $P_{ef}$ can be more than doubled, demonstrating a huge performance upgrade when Scheme III was adopted. Unexpectedly, fan sizes exerts limited influence on $P_{ef}$ under the same ACH with a standard fan performing slightly better than a larger fan. This is because a smaller fan can obtain a faster air suction flow due to mass conservation. At the beginning of the flushing-induced plume where the particle distribution is relatively concentrated, a local stronger suction flow velocity gained by a smaller fan can absorb a large number of newly rising aerosols. Although the large fan can have a larger absorption flow area, its suction flow velocity is lower compared to a smaller fan for a given ACH. That means a weakened local suction capability, where a plenty of aerosols fail to be absorbed by the fan, indicating a relatively low $P_{ef}$. In addition, Fig. 8C shows that the proportions of particles attaching to the standing human $P_{man}$ can be reduced from ~ 4.40% to ~ 0.100% when the ACH boosts from 6 to 40 $h^{-1}$.

Supplementary material related to this article can be found online at doi:10.1016/j.jhazmat.2022.129697.

### 3.2. Experimental results

Simulation results were verified by experiments as shown in Fig. 9. Fig. 9A and B demonstrate the smoke dynamics in Schemes I and III. The still smoke patterns at time elapsed of 1.00, 10.0, and 30.0 s in Schemes III are shown in Fig. 9A. From the beginning to the time of 30.0 s, the ascending smoke could be driven and controlled by the fan suction flow (as shown in the red dotted arrows in Fig. 9A), which can prevent the smoke from spreading through the bathroom space. (Please see Movie S4 for the full process of the smoke removal in Scheme III). Here it could be observed that almost all of the smoke was removed by the side fan after one minute from the time of flushing. However, the smoke dynamics in Scheme I, illustrated in Fig. 9B, was different where the smoke could be diffused horizontally from the start (See Fig. 9B at the time elapsed of 1.00 s) although the ceiling fan was operating. When the time elapsed reached 5.00 s, there was also a clear horizontal flow, suggesting an additional large probability of aerosol propagation. As time

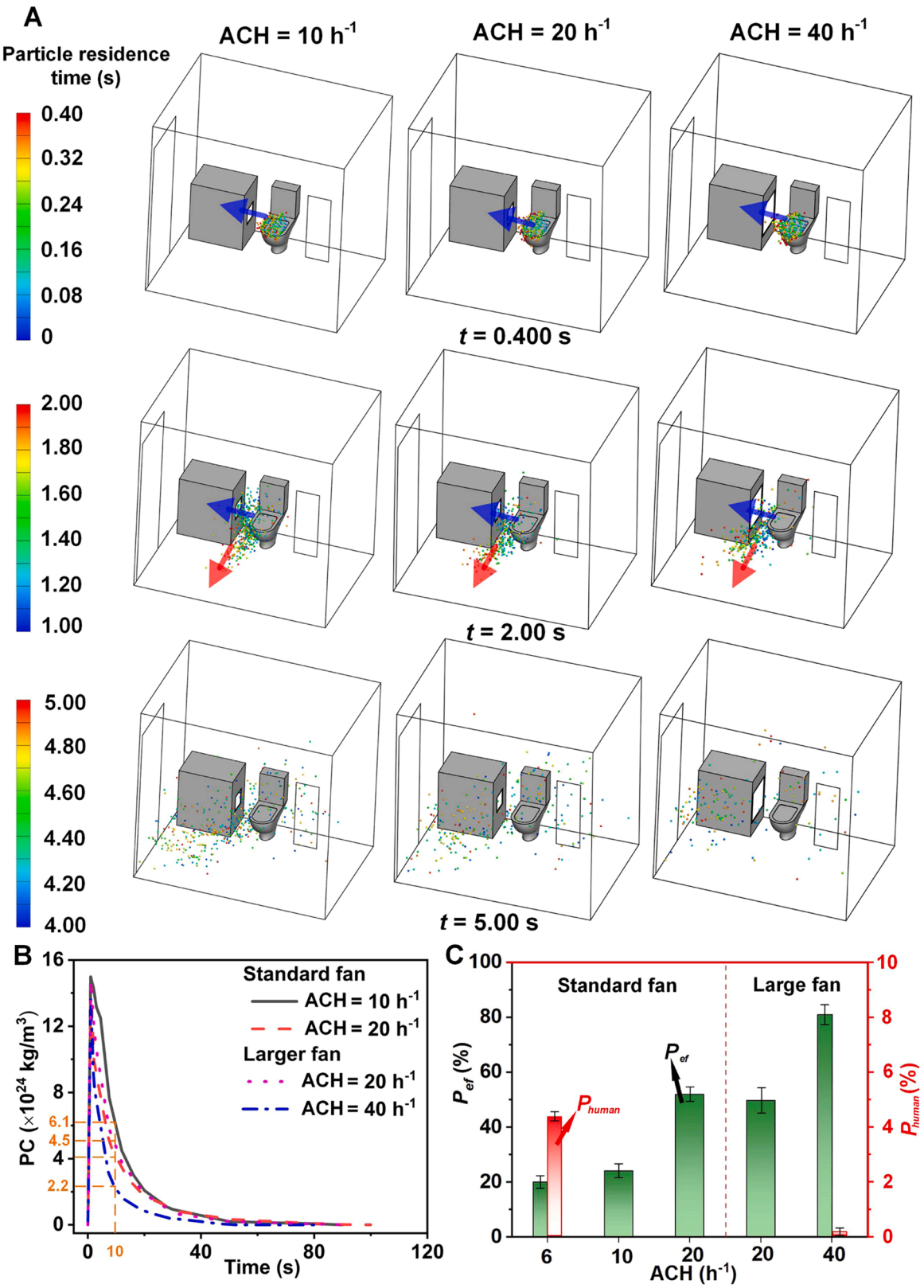


**Fig. 8.** Aerosol particle movement and concentration dynamics in Scheme III. (A) Aerosol Particle movements at different time (0–5.00 s) for various ACHs. (B) Aerosol particle concentration dynamics in the bathroom. (C) Comparisons of proportions of particles escaping from the fan and attaching to the human for various ACHs.

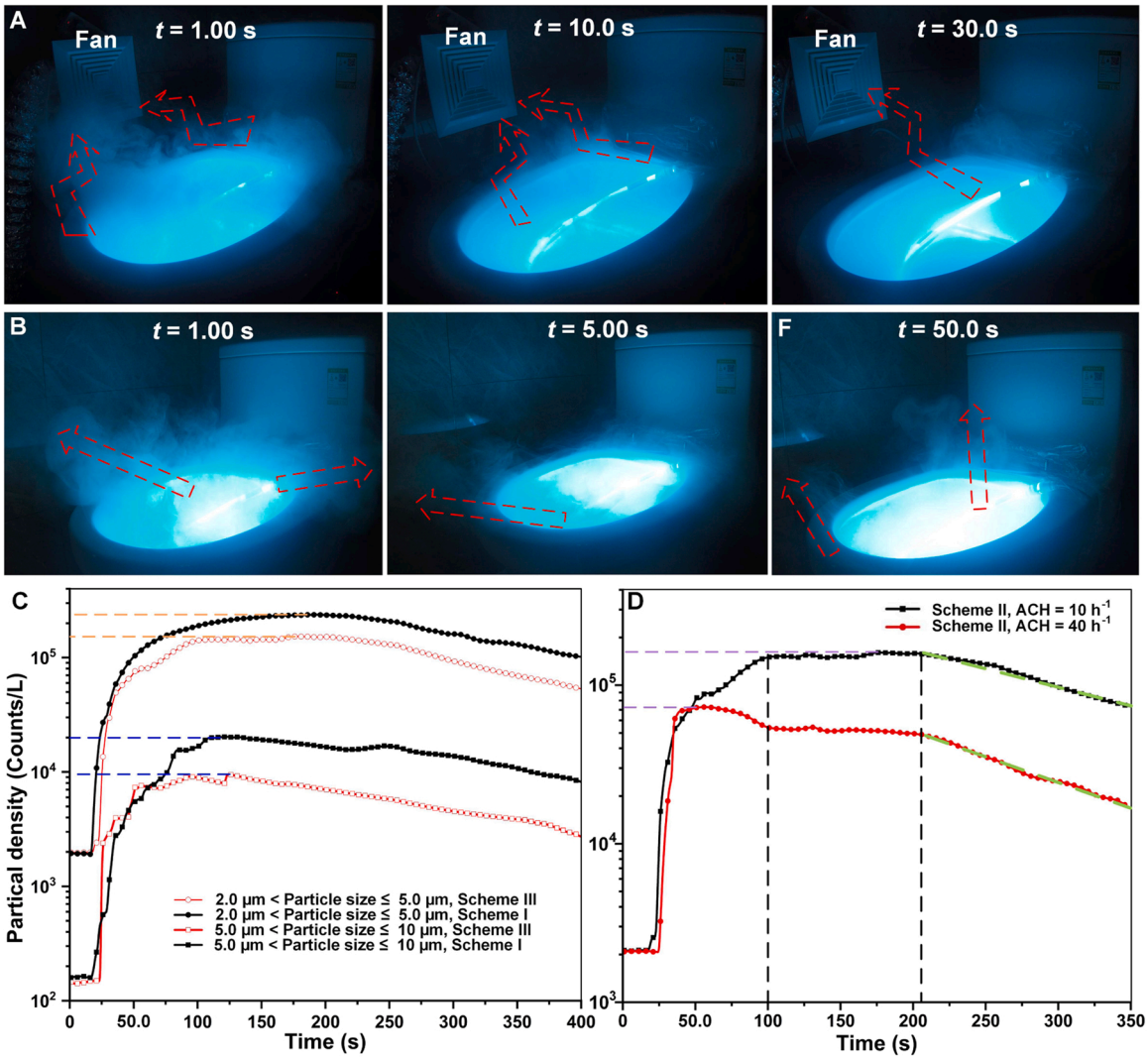


**Fig. 9.** Experimental results of the smoke-assisted experimental results. (A) Visual images of smoke dynamics after flushing in Scheme III at ACH of 10 $h^{-1}$. (B) Visual images of smoke dynamics after flushing in Scheme I at ACH of 10 $h^{-1}$. (C) Comparison of particle density dynamics between Scheme I and III. (D) Comparison of particle density dynamics (the particle size between 2.0 and 10 μm was counted as a whole) between two ACHs (10 and 40 $h^{-1}$) in Scheme III. The time in (A) and (B) is the time elapsed after the flushing button was pressed. The two green dotted line in (D) are guides for clearer viewing.

elapsed approached 50.0 s, there was still smoke ascending from the toilet, suggesting a weak removal ability of the ceiling fan in Scheme I. (Please review Movie S5 for the full process of the smoke removal in Scheme I where there still was a large amount of smoke inside and above the toilet space even after two minutes after the toilet was flushed).

Supplementary material related to this article can be found online at doi:10.1016/j.jhazmat.2022.129697.

Fig. 9C and D show the particle density dynamics during the smoke-assisted experiment. In Fig. 9C particle sizes of between 2.0 and 5.0 μm and between 5.0 and 10 μm were counted separately under Schemes I and III. Here the curves experience clear increases at the time elapsed of ~ 25.0 s, which suggested the spread of flushing-induced aerosol particles. As expected, the particle densities in Scheme I were generally higher than those in Scheme III. The density of bigger particles (5.0–10 μm) increased from ~ 150 (in both Schemes I and III) to 20,251.2 (in Scheme I) and 9516.50 (in Scheme III) counts/L, which was the highest during the experiments for the certain particle size range. Therefore, a 53.0% reduction in density of the bigger particles could be achieved when Scheme III was applied. The highest particle density of the smaller particle (2.0–5.0 μm) for Schemes I and III were counts of 237,660 and 151,996 counts/L, whereby a 36.0% reduction was attained. By comparing the statistical data, aerosol particle removal capability clearly increased when Scheme III is applied. Fig. 9D shows the ACH effect in Scheme III. When compared to the performance under the ACH of 10 $h^{-1}$, the 40 $h^{-1}$ ACH could rapidly control the particle density as the red curve in Fig. 9D dropped quickly (at 50 s) after a sudden boost at 25.0 s. However, the elevating trend lasted until the time elapsed was 100 *s* for the ACH of 10 $h^{-1}$. The biggest particle density count for the 40 $h^{-1}$ ACH was 73,932.4 counts/L, attaining a 54.0% reduction compared to that of the ACH of 10 $h^{-1}$. A similar steady phase occurred for both these ACHs as shown by the two vertical dashed lines from 50.0 to 210 s, where the particle density remained almost constant. The particle density for the low ACH was maintained at a high level at its highest value, while that for the high ACH retained a secondary high position which experienced a clear drop. After the steady phase, both curves descend linearly at a steady rate (shown here by two green dashed lines).

## 4. Discussion

Although disease transmissions in family bathrooms and public restrooms are difficult to quantify due to the lack of surveillance and related environmental data for epidemiologists, multiple sources have verified and reported mass cross-infections of COVID-19 in bathrooms

and restrooms via a vertical transmission pattern (the chimney effect). This is especially the case in densely populated areas, leading to large-scale community outbreaks of COVID-19. In order to minimize the vertical transmission in bathrooms, the utilization of disinfection tablets in the drainage system is recommended. However, the effectiveness of such measures has not yet been fully investigated (Buonerba et al., 2021), and neither has the sustainability (Cui et al., 2022; Kumar et al., 2021; Lou et al., 2021). Moreover, many publications have shown that the enveloped viruses like SARS-Cov-2, wrapped by organic materials as they are, can survive the disinfection (Bogler et al., 2020; Ye et al., 2016; Geller et al., 2012). In this paper, we systematically investigated the location and exhaust rate effect on the ventilation fan effectiveness in a typical bathroom space, and have offered more sustainable approaches according as identified by our research.

We were able to show that the ceiling exhaust fan in the traditional bathroom ventilation (Scheme I in this paper) failed to function effectively by using both computational and experimental approaches. Using CFD, we have demonstrated that a main horizontal airflow can disturb the suction flow effect of the ceiling fan in which the majority of the ascending aerosol particles are not extracted by the ceiling fan even when boosting the ACH, which is suggested with the current infection control guideline. Therefore, traditional bathroom ventilation needs to be altered and improved accordingly to guarantee human occupants a safe and sustainable family-based built environment, especially during public health crises such as the COVID-19 outbreak. We first placed the fan on the floor (in Scheme II) which brought better performances. Although still affected by horizontal airflow, the suction flow from the floor fan could exert enough of an effect on the lifted aerosols from the toilet bowl, whereby the particle dynamic simulation demonstrated a significant improvement where $P_{ef}$ could be above 10.2%, compared to nearly zero in traditional ventilation schemes. However, the bathroom is a wet area where a floor fan could cause unsafe circuit hazards. When a fan is deployed in a side wall (see Scheme III) next to the cabinet, an even better performance could be attained. Here $P_{ef}$ could reach 80.9% when the ACH is regulated to perform at 40 $h^{-1}$, which obtained a 163% increase compared with that of the floor fan extraction. Aerosol removal capability in bathrooms is thus expected to improve accordingly. Nevertheless, in our simulations, we have not considered potential effects such as the hazardous plume from the floor drain, or the air flow caused by human behaviors.

We conducted experiments to validate the removal of aerosols. Here we used smoke visualization technology and a particle counter to compare further the particle removal capabilities of ventilation Schemes I and III. Weaker smoke absorption and higher particle density during the experiments were observed in Scheme I compared to those of Scheme III, which suggested that there is an urgency in the reconstruction of bathroom ventilation systems. Our results have indicated that simply enhancing the exhaust air volume in the bathroom under the traditional scheme offers little help. However, enhancing ventilation capability by boosting ACH from 10 to 40 $h^{-1}$ can make a difference when Scheme III is applied. Although Scheme III can fundamentally accelerate the dilution effect, the particle density remained at a relatively high level (the steady phase in Fig. 8D from 100 to ~ 210 s) even under the highest ACH conditions. It thus is recommended that a proper time interval between two toilet users should be at least ~ 210 s to avoid the phase with a relatively high particle density in the air. These findings suggested that our proposed bathroom reconstruction could not only dilute the hazardous floated aerosol particles in the bathroom but also minimize exposure to such particles in even bigger indoor environments that are connected to the bathroom space. Data in this paper also clearly demonstrated possible cross-infection even in the recommended ventilation scheme, where it can only reduce the infection probability but not eliminate this risk entirely.

The COVID-19 crisis has reflected the fragility of the modern medical system that has been established by advanced medical science, technology, and well-trained medical professionals due to massive and uncontrolled community-wide cross-infections. People may have a choice not to go to sports centers, restaurants, gyms, or other public areas but they have no choice but to stay at home, and do so to minimize the probability of infection during a pandemic. However, constant community outbreaks have made the number of infected cases increase markedly across the world, overwhelming local medical resources (Wilson et al., 2022) and evolving into a global pandemic crisis. Thus, finding ways to break the transmission chain in the community efficiently should be critical to reduce the incidence of COVID-19 and similar viral outbreaks. Vertical transmission in high-rise buildings is highly significant as people can be infected without direct contact with the originally infected person, making family indoor environments unsafe. Indeed, contactless infections in communities especially in vertically-aligned apartments with shared drainage systems have been identified before. Traditional ceiling fans have proven to be ineffective in reducing aerosols, and thus ventilation reconstruction via changing the fan location is a more efficient approach according to the findings in this paper. Moreover, not only for the SARS-Cov-2 outbreak, but the proposed ventilation reconstruction could also prevent community-based vertical disease transmission caused by other viruses or bacterium that are transmitted via human to human transmissions such as SARS-CoV (Ding et al., 2004), MERS-CoV (Drosten et al., 2013), Hepatitis (Mollalo et al., 2021), adenovirus (Gude and Muire, 2021), Salmonella (Xie et al., 2020)' and other emerging pathogens.

## 5. Conclusions

Family bathroom fan location, size, flow rate, and flow velocity effects on the aerosol removal and distribution were investigated quantitatively and visually in this paper. Key conclusions are summarized as follows:

- Traditional ceiling fan even with an enhanced ventilation capability fails to remove hazardous plume from toilets in bathrooms.
- A side-wall fan has an efficient aerosol removal capability.
- An enhanced ventilation capability for the side-wall fan can increase the aerosol absorption ability significantly where $P_{ef}$ can be increased by 236% when ACH is increased from 10 to 40 $h^{-1}$.
- For a given ventilation flow rate, a smaller fan in the market is preferred if its noise is within the acceptable range.
- Bathroom ventilation reconstructions are encouraged to be performed accordingly.

The practical implications of this paper are thus summarized as follows: (1). Using visualization techniques, this paper can guide the public to rethink the bathroom construction and family-based infection control guidelines, as well as urge them to reconstruct bathrooms and smart ventilation systems in a more scientific way rather than the traditional approach; (2). Rethink in the construction of public health quarantine facilities and their bathroom reconstructions are recommended to be implemented immediately in centralized-quarantined high-rise buildings; (3). More attention (like stricter personal protection and more frequent nucleic acid testing) should be paid to ensure worker hygiene in public restrooms as long-term exposure to infectious aerosols can increase infection probability significantly. (4). The public should be encouraged to report their access to public restrooms via possibly scanning code for rapid risk identification and epidemiological track. The implications raised here could contribute to the construction of more sustainable, smarter, and healthier buildings, preparing residents more effectively in confronting emerging and re-emerging pandemics.

## Environmental implication

Environmental transmissions of COVID-19 in densely populated areas due to the hazardous vertical chimney effect have been not only reported by journalists intensively but also verified by epidemiologists

and fluid experts extensively. We specifically studied the performance of current-recommended infection-prevention measurements and found it barely works for preventing the chimney-effect-induced environmental transmission pattern. Accordingly, we found a more efficient risk mitigation strategy that can minimize the vertical transmission risk. Through visualization technology and solid evidence, this study proposes bathroom ventilation reconstruction and promotes a safe and sustainable built environment.

## CRediT authorship contribution statement

JW and SY conceptualized the study. JW, ZW and HW conducted the experiments. MZ and YM guided the implementation of the experimentation. JW, HW, and YL conducted the simulation. JW and MW verified the data used in both the simulation and experiment. SY supervised the study and reviewed and edited the final version of the manuscript. All authors wrote the manuscript and approved the submission of the manuscript.

## Declaration of Competing Interest

The authors declare that they have no known competing financial interests or personal relationships that could have appeared to influence the work reported in this paper.

## Data Availability

Data will be made available on request. The data that supports the findings of this study are available within the article and its supplementary material.

## Acknowledgment

This work was supported by the National Natural Science Foundation of China (No. 52106114).

## Appendix A. Supplementary material

Supplementary data associated with this article can be found in the online version at doi:10.1016/j.jhazmat.2022.129697.

## References

Ali, W., Zhang, H., Wang, Z., Chang, C., Javed, A., Ali, K., Du, W., Niazi, N.K., Mao, K., Yang, Z., 2021. Occurrence of various viruses and recent evidence of SARS-CoV-2 in wastewater systems. J. Hazard. Mater. 414, 125439.

ASHRAE, 2013. ASHRAE Fundamental S1 Handbook. Atlanta, GA.

ASHRAE, 2020. ASHRAE issues statements on relationship between COVID-19 and HVAC in buildings. ⟨https://www.ashrae.org/about/news/2020/ashrae-issues-statements-on-relationship-between-covid-19-and-hvac-in-buildings⟩. (Accessed 22 July 2020).

Bogler, A., Packman, A., Furman, A., Gross, A., Kushmaro, A., Ronen, A., 2020. Rethinking wastewater risks and monitoring in light of COVID-19 pandemics. Nat. Sustain. 3, 981–990.

Bourouiba, L., 2020. Turbulent gas clouds and respiratory pathogen emissions: potential implications for reducing transmission of COVID-19. J. Am. Med. Assoc. 323, 1837–1838.

Bourouiba, L., 2021. The fluid dynamics of disease transmission. Annu. Rev. Fluid Mech. 53, 473–508.

Bourouiba, L., Dehandschoewercker, E., Bush, J.W.M., 2014. Violent expiratory events: on coughing and sneezing. J. Fluid Mech. 745, 537–563.

Breaking Latest News, 2021. Guangzhou Has A Shortest 14-second Transmission Case: Delta Strain Infection Is Faster, and Existing Vaccines Are Effective - Warning! ⟨https://www.breakinglatest.news/tag/the-shortest-14-second-transmission-case-in-guangzhou-delta-strain-infection-is-faster-and-existing-vaccines-are-effective⟩. (Accessed 24 June 2021).

Buonerba, A., Corpuz, M.V.A., Ballesteros, F., Choo, K.-H., Hasan, S.W., Korshin, G.V., et al., 2021. Coronavirus in water media: analysis, fate, disinfection and epidemiological applications. J. Hazard. Mater. 415, 125580.

Cable News Network, 2020. Woman May Have Caught Coronavirus in Airplane Toilet, Researchers Say. ⟨https://edition.cnn.com/2020/08/26/health/coronavirus-passenger-toilet-korea/index.html⟩. (Accessed 26 August 2020).

Cao, X., Hao, G., Li, Y., Wang, M., Wang, J., 2022. On male urination and related environmental disease transmission in restrooms: from the perspectives of fluid dynamics. Sustain. Cities Soc. 80, 103753.

Catalina, T., Iordache, V., Iordache, F., 2020. Correlation between air and sound propagation to determine air permeability of buildings for single/double wood pane windows. Energ. Build. 224, 110253.

Cheng, P., Luo, K., Xiao, S., Yang, H., Hang, J., Ou, C., Cowling, B.J., Yen, H.L., Hui, D., Hu, S., Li, Y., 2022a. Predominant airborne transmission and insignificant fomite transmission of SARS-CoV-2 in a two-bus COVID-19 outbreak originating from the same pre-symptomatic index case. J. Hazard. Mater. 425, 128051.

Cheng, V.C., Lung, D.C., Wong, S. –C., Au, A.K., Wang, Q., Chen, H., et al., 2022b. Outbreak investigation of airborne transmission of Omicron (B.1.1.529) - SARS-CoV-2 variant of concern in a restaurant: implication for enhancement of indoor air dilution. J. Hazard. Mater. 430, 128504.

Cui, H., Zhu, X., Zhu, Y., Huang, Y., Chen, B., 2022. Ecotoxicological effects of DBPs on freshwater phytoplankton communities in co-culture systems. J. Hazard. Mater. 421, 126679.

Dancer, S.J., Li, Y., Hart, A., Tang, J.W., Jones, D.L., 2021. What is the risk of acquiring SARS-CoV-2 from the use of public toilets? Sci. Total Environ. 792, 148341.

Dbouk, T., Drikakis, D., 2020. On coughing and airborne droplet transmission to humans. Phys. Fluids 32, 05330.

Dbouk, T., Drikakis, D., 2021. On airborne virus transmission in elevators and confined spaces. Phys. Fluids 33, 011905.

Ding, Y., He, L., Zhang, Q., Huang, Z., Che, X., Hou, J., et al., 2004. Organ distribution of severe acute respiratory syndrome (SARS) associated coronavirus (SARS-CoV) in SARS patients: Implications for pathogenesis virus transmission pathways. J. Pathol. 203, 622–630.

Drosten, C., Seilmaier, M., Corman, V.M., Hartmann, W., Scheible, G., Sack, S., et al., 2013. Clinical features and virological analysis of a case of Middle East respiratory syndrome coronavirus infection. Lancet Infect. Dis. 13, 745–751.

Feng, B., Xu, K., Gu, S., Zheng, S., Zou, Q., Xu, Y., et al., 2021. Multi-route transmission potential of SARS-CoV-2 in healthcare facilities. J. Hazard. Mater. 402, 123771.

Fennelly, K.P., 2020. Particle sizes of infectious aerosols: implications for infection control. Lancet Resp. Med. 8, 914–924.

Geller, C., Varbanov, M., Duval, R.E., 2012. Human coronaviruses: insights into environmental resistance and its influence on the development of new antiseptic strategies. Viruses 4, 3044–3068.

Global Times, 2020. Two of Beijing's COVID-19 Cases Infected from A Public Toilet. ⟨https://www.globaltimes.cn/content/1192683.shtml⟩. (Accessed 26 June 2020).

Gude, V.G., Muire, P.J., 2021. Preparing for outbreaks - implications for resilient water utility operations and services. Sustain. Cities Soc. 64, 102558.

Guo, M., Tao, W., Flavell, R.A., Zhu, S., 2021. Potential intestinal infection and faecal–oral transmission of SARS-CoV-2. Nat. Rev. Gastroenterol. Hepatol. 18, 269–283.

Huang, W., Wang, K., Hung, C.-T., Chow, K.-M., Tsang, D., Lai, R.W.-M., et al., 2022. Evaluation of SARS-CoV-2 transmission in COVID-19 isolation wards: on-site sampling and numerical analysis. J. Hazard. Mater. 436, 129152.

Hwang, S.E., Chang, J.H., Oh, B., Heo, J., 2021. Possible aerosol transmission of COVID-19 associated with an outbreak in an apartment in Seoul, South Korea, 2020. Int. J. Infect. Dis. 104, 73–76.

Kang, M., Wei, J., Yuan, J., Guo, J., Zhang, Y., Hang, J., Qu, Y., Qian, H., Zhuang, Y., Chen, X., Peng, X., Shi, T., Wang, J., Wu, J., Song, T., He, J., Li, Y., Zhong, N., 2020. Probable evidence of fecal aerosol transmission of SARS-CoV-2 in a high-rise building. Ann. Intern. Med. 173, 974–980.

Kanso, M.A., Piette, J.H., Hanna, J.A., Giacomin, A.J., 2020. Coronavirus rotational diffusivity. Phys. Fluids 32, 123101.

Kong, X., Guo, C., Lin, Z., Duan, S., He, J., Ren, Y., Ren, J., 2021. Experimental study on the control effect of different ventilation systems on fine particles in a simulated hospital ward. Sustain. Cities Soc. 73, 103102.

Kumar, M., Dhangar, K., Thakur, A.K., Ram, B., Chaminda, T., Sharma, P., et al., 2021. Antidrug resistance in the Indian ambient waters of Ahmedabad during the COVID-19 pandemic. J. Hazard. Mater. 416, 126125.

Kutralam-Muniasamy, G., Pérez-Guevara, F., Shruti, V.C., 2022. A critical synthesis of current peer-reviewed literature on the environmental and human health impacts of COVID-19 PPE litter: new findings and next steps. J. Hazard. Mater. 422, 126945.

Li, Y., Qian, H., Hang, J., Chen, X., Cheng, P., Ling, H., et al., 2021. Probable airborne transmission of SARS-CoV-2 in a poorly ventilated restaurant. Build. Environ. 196, 107788.

Li, Y.Y., Wang, J.X., Chen, X., 2020. Can a toilet promote virus transmission? From a fluid dynamics perspective. Phys. Fluids 32, 065107.

Liu, X., Dou, Z., Wang, L., Su, B., Jin, T., Guo, Y., et al., 2022. Close contact behavior-based COVID-19 transmission and interventions in a subway system. J. Hazard. Mater. 436, 129233.

Liu, Y., Ning, Z., Chen, Y., Guo, M., Liu, Y., Gali, N.K., 2020. Aerodynamic analysis of SARS-CoV-2 in two Wuhan hospitals. Nature 582, 557–560.

Lou, J., Wang, W., Lu, H., Wang, L., Zhu, L., 2021. Increased disinfection byproducts in the air resulting from intensified disinfection during the COVID-19 pandemic. J. Hazard. Mater. 418, 126249.

Lu, R., Zhao, X., Li, J., Niu, P., Yang, B., Wu, H., et al., 2020. Genomic characterization and epidemiology of 2019 novel coronavirus: implications for virus origins and receptor binding. Lancet 395, 565–574.

Mesgarpour, M., Abad, J.M.N., Alizadeh, R., Wongwises, S., Doranehgard, M.H., Ghaderi, S., Karimi, N., 2021. Prediction of the spread of Corona-virus carrying droplets in a bus - a computational based artificial intelligence approach. J. Hazard. Mater. 413, 125358.

Mirzaie, M., Lakzian, E., Khan, A., Warkiani, M.E., Mahian, O., Ahmadi, G., 2021. COVID-19 spread in a classroom equipped with partition – a CFD approach. J. Hazard. Mater. 420, 126587.
Mollalo, A., Rivera, K.M., Vahabi, N., 2021. Spatial statistical analysis of pre-existing mortalities of 20 diseases with COVID-19 mortalities in the continental United States. Sustain. Cities Soc. 67, 102738.
Moritz, S., Gottschick, C., Horn, J., Popp, M., Langer, S., et al., 2021. The risk of indoor sports and culture events for the transmission of COVID-19. Nat. Commun. 12, 5096.
Narayanan, S.R., Yang, S., 2021. Airborne transmission of virus-laden aerosols inside a music classroom: effects of portable purifiers and aerosol injection rates. Phys. Fluids 33, 033307.
Nicas, M., Nazaroff, W.W., Hubbard, A., 2005. Toward understanding the risk of secondary airborne infection: emission of respirable pathogens. J. Occup. Environ. Hyg. 2, 143–154.
Park, J., Lee, K.S., Park, H., 2022a. Optimized mechanism for fast removal of infectious pathogen-laden aerosols in the negative-pressure unit. J. Hazard. Mater. 435, 128978.
Park, J.Y., Mistur, E., Kim, D., Mo, Y., Hoefer, R., 2022b. Toward human-centric urban infrastructure: text mining for social media data to identify the public perception of COVID-19 policy in transportation hubs. Sustain. Cities Soc. 76, 103524.
Peng, L., Liu, J., Xu, W.X., Luo, Q.M., Chen, D.B., Lei, Z.Y., 2020. SARS-CoV-2 can be detected in urine, blood, anal swabs, and oropharyngeal swabs specimens. J. Med. Virol. 92, 1676–1680.
Peng, Z., Pineda Rojas, A.L., Kropff, E., Bahnfleth, W., et al., 2022. Practical indicators for risk of airborne transmission in shared indoor environments and their application to COVID-19 outbreaks. Environ. Sci. Technol. 56, 1125–1137.
Schreck, J.H., Lashaki, M.J., Hashemi, J., Dhanak, M., Verma, S., 2021. Aerosol generation in public restrooms. Phys. Fluids 33, 033320.
Seller, V.T., Brilliant, C.D., Morgan, C., Lewis, S.P., Duckers, J., Boy, F.A., Lewis, P.D., 2021. Anti-perspirant deodorant particulate matter temporal concentrations during home usage. Build. Environ. 195, 107738.
Shao, S., Zhou, D., He, R., Li, J., Zou, S., Mallery, K., Kumar, S., Yang, S., Hong, J., 2021. Risk assessment of airborne transmission of COVID-19 by asymptomatic individuals under different practical settings. J. Aerosol Sci. 151, 105661.
Sheikhnejad, Y., Aghamolaei, R., Fallahpour, M., Motamedi, H., Moshfeghi, M., Mirzaei, P.A., Bordbar, H., 2022. Airborne and aerosol pathogen transmission modeling of respiratory events in buildings: an overview of computational fluid dynamics. Sustain. Cities Soc. 79, 103704.
Shih, T.H., Liou, W.W., Shabbir, A., Yang, Z., Zhu, J., 1995. A new k-$\epsilon$ eddy viscosity model for high reynolds number turbulent flows. Comput. Fluids 24, 227–238.
Tang, J.W., Marr, L.C., Li, Y., Dancer, S.J., 2021. Covid-19 has redefined airborne transmission. BMJ 373, n913.
Tencent News, 2022. An Infection during a One-month Isolation at Home (in Chinese). ⟨https://new.qq.com/omn/20220426/20220426A0DR0200.html⟩. (Accessed 26 April 2022).
Tran, H.N., Le, G.T., Nguyen, D.T., Juang, R.S., Rinklebe, J., Bhatnagar, A., et al., 2021. SARS-CoV-2 coronavirus in water and wastewater: a critical review about presence and concern. Environ. Res. 193, 110265.
Wade, M.J., Jacomo, A.L., Armenise, E., Brown, M.R., Bunce, J.T., Cameron, G.J., et al., 2022. Understanding and managing uncertainty and variability for wastewater monitoring beyond the pandemic: lessons learned from the United Kingdom national COVID-19 surveillance programmes. J. Hazard. Mater. 424, 127456.
Wang, Q., Liu, L., 2021. On the critical role of human feces and public toilets in the transmission of COVID-19: Evidence from China. Sustain. Cities Soc. 75, 103350.
Wang, C.C., Prather, K.A., Sznitman, J., Jimenez, J.L., Lakdawala, S.S., Tufekci, Z., Marr, L.C., 2021a. Airborne transmission of respiratory viruses. Science 373, eabd9149.
Wang, J.X., Cao, X., Chen, Y.P., 2021b. An air distribution optimization of hospital wards for minimizing cross-infection. J. Clean. Prod. 279, 123431.
Wang, J.X., Guo, W., Xiong, K., Wang, S.N., 2020b. Review of aerospace-oriented spray cooling technology. Prog. Aerosp. Sci. 116, 100635.
Wang, J., Huang, J., Fu, Q., Gao, E., Chen, J., 2022a. Metabolism-based ventilation monitoring and control method for COVID-19 risk mitigation in gymnasiums and alike places. Sustain. Cities Soc. 80, 103719.
Wang, J.X., Li, Y.Y., Liu, X.D., Cao, X., 2020a. Virus transmission from urinals. Phys. Fluids 32, 081703.
Wang, J., Li, Y., Liu, X., Shen, C., Zhang, H., Xiong, K., 2021c. Recent active thermal management technologies for the development of energy-optimized aerospace vehicles in China. Chinese J. Aeronaut. 34, 1–27.
Wang, Q., Li, Y., Lung, D.C., Chan, P., Dung, C., Jia, W., et al., 2022b. Aerosol transmission of SARS-CoV-2 due to the chimney effect in two high-rise housing drainage stacks. J. Hazard. Mater. 421, 126799.
Wang, Q., Lin, Z., Niu, J., Choi, G.K., Fung, J.C.H., Lau, A.K.H., et al., 2022c. Spread of SARS-CoV-2 aerosols via two connected drainage stacks in a high-rise housing outbreak of COVID-19. J. Hazard. Mater. 430, 128475.
Wilson, A.M., Sleeth, D.K., Schaefer, C., Jones, R.M., 2022. Transmission of respiratory viral diseases to health care workers: COVID-19 as an example. Annu. Rev. Public Health 43, 311–330.
Wu, S.-C., Guo, M.-Y., Wang, J.-X., Yao, S., Chen, J., Li, Y.Y., 2020. Liquid-curtain-based strategy to restrain plume during flushing. Phys. Fluids 32, 111707.
Wu, L., Liu, X., Yao, F., Chen, Y., 2021. Numerical study of virus transmission through droplets from sneezing in a cafeteria. Phys. Fluids 33, 023311.
Xie, S., Jiang, L., Wang, M., Sun, W., Yu, S., Turner, J.R., Yu, Q., 2020. Cadmium ingestion exacerbates Salmonella infection, with a loss of goblet cells through activation of Notch signaling pathways by ROS in the intestine. J. Hazard. Mater. 391, 122262.
Yang, X., Ou, C., Yang, H., Liu, L., Song, T., Kang, M., et al., 2020. Transmission of pathogen-laden expiratory droplets in a coach bus. J. Hazard. Mater. 397, 122609.
Yao, F., Liu, X., 2021. The effect of opening window position on aerosol transmission in an enclosed bus under windless environment. Phys. Fluids 33, 123301.
Ye, Y., Ellenberg, R.M., Graham, K.E., Wigginton, K.R., 2016. Survivability, partitioning, and recovery of enveloped viruses in untreated municipal wastewater. Environ. Sci. Technol. 50, 5077–5085.
Yu, H., Ye, X., Zhang, M., Zhang, F., Li, Y., Pan, S., Li, Y., Yu, H., Lu, C., 2021. Study of SARS-CoV-2 transmission in urban environment by questionnaire and modeling for sustainable risk control. J. Hazard. Mater. 420, 126621.
Yu, H.C., Mui, K.W., Wong, L.T., Chu, H.S., 2017. Ventilation of general hospital wards for mitigating infection risks of three kinds of viruses including Middle East respiratory syndrome coronavirus. Indoor Built Environ. 26, 514–527.
Yu, I.T., Li, Y., Wong, T.W., Tam, W., Chan, A.T., Lee, J.H., Leung, D.Y., Ho, T., 2004. Evidence of airborne transmission of the severe acute respiratory syndrome virus. N. Engl. J. Med. 350, 1731–1739.
Zheng, K., Ortner, P., Lim, Y.W., Zhi, T.J., 2021. Ventilation in worker dormitories and its impact on the spread of respiratory droplets. Sustain. Cities Soc. 75, 103327.